Preliminary Studies on the Design and Simulation of High Resolution Small Animal PET Scanners with Octagonal Geometry

Juan E. Ortuño, Juan J. Vaquero, *Senior Member, IEEE*, George Kontaxakis, *Member, IEEE*, Manuel Desco, and Andrés Santos, *Senior Member, IEEE*

Abstract – We present a preliminary study on the design of a small animal positron emission tomograph with octagonal geometry. The main goal is to evaluate the impact of critical design parameters on the quality of the reconstructed images. Monte Carlo simulations take into account the depth of interaction in individual crystals. The activity sources are simulated as parametric distributions within the field of view and images are reconstructed with iterative algorithms based on the estimation of maximum likelihood and Bayesian regularization. The probability system matrix used by these algorithms is also calculated based on statistical models and Monte Carlo simulation. 2D and 3D techniques have been employed.

I. Introduction

In the last few years there is a strong interest in applying non-invasive imaging techniques on small animals like rats and mice, widely used in biomedical and pharmacological research and studies of different human diseases. Positron emission tomography (PET) is a molecular imaging modality that permits the study of biochemical processes through the use of positron-labeled molecular probes. This technique has been adapted to image small animals, mainly by miniaturizing designs of PET scanners for humans [1].

For crystal-based tomographs the sensitivity is highly dependent on the crystal size and the smaller dimensions of the volumes under study make necessary a high spatial resolution. Although the sensitivity and resolution limits are primarily imposed by the detector technology [2], the scanner geometry and appropriate image reconstruction methods can significantly improve the performance of small animal PET scanners.

In this work we propose an octagonal scanner configuration, which can achieve a good intrinsic sensitivity based on a simple design. Attention is paid to the effect of gaps between detector blocks in the produced images.

II. Tomograph Geometry

The basic design of the proposed tomograph consists of eight detector blocks that form a regular octagon (figure 1a,b). Each detector is formed by a pixelized crystal array made of scintillator material, connected to a large area position-sensitive photomultiplier tube (PS-PMT) [3].

Coincidences are allowed between one block and the three opposites, resulting in a total of twelve possible detector block pairs in coincidence. The block separation distance and the number of crystals in a block are adjusted in the optimization process. In this geometry, without bed or gantry rotation, it is not possible to obtain complete projections in the whole field of view (FOV).

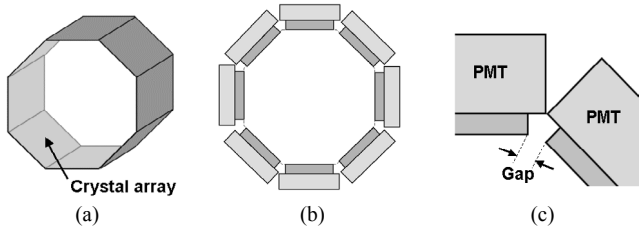

Fig. 1. (a) Octagonal geometry: eight detectors form a regular octagon in the axial plane. (b) Transaxial view of the scanner configuration, each octagon side is made of an array of scintillation crystals attached to a photomultiplier tube. (c) Detail of a gap between detectors.

The size of the detectors blocks and their separation determines an angular gap among them (figure 1c). Their presence creates areas without registered activity in the rebinned sinograms (figure 2a). Furthermore, valid coincidences (figure 2b) can go undetected.

Given a detector block size, the minimum separation between opposite detectors occurs when the crystal arrays completely cover the sides of the octagon. In this case there are no physical gaps between consecutive detectors, although lower sensitivity corresponds to the areas at the junctions between blocks. The FOV can be modified by changing the separation between detector blocks, but at the expense of larger gaps and decreasing sensitivity.

III. Monte Carlo Simulation

In order to analyze the sensitivity and spatial resolution of the proposed tomograph configuration, as well as to study the reconstruction algorithms adapted to this geometry, a 3D

0-7803-8257-9/04/$20.00 © 2004 IEEE.

simulator based on Monte Carlo techniques has been implemented. The simulator models positron range, non colinearity and depth of interaction (DOI) in crystal. Since a high number of recorded annihilation events are needed for realistic simulations, the current version of the simulator does not simulate scattering and attenuation.

The activity within the source can be defined by several classes of parametric volumes within the FOV or specific distributions defined for each voxel. To reduce computing, the γ-rays can be generated uniformly solely in directions within the solid angle of coincidences allowed.

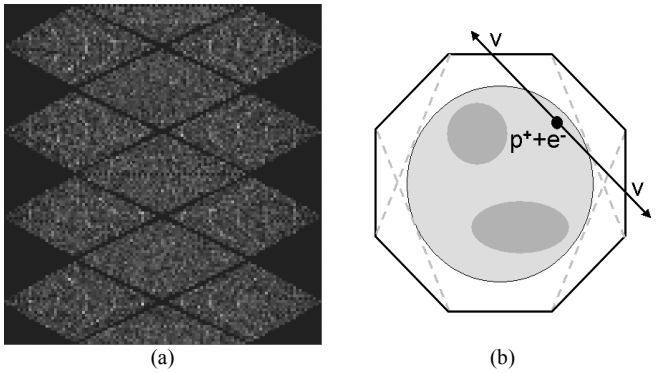

Fig. 2. (a) 2D sinogram without corrections, resulting from a uniform activity within the FOV; (b) example of a valid coincidence event within the FOV, which does not get registered by the scanner's coincidence electronics.

The simulated data is initially stored in histogram mode. For sinogram-based reconstruction algorithms, the coincidence data stored in histogram mode is rebinned into direct and oblique sinograms, similar to those proposed by Defrise, *et al.* [4] for cylindrical geometries. In octagonal configurations without rotation, sinograms present characteristically rhomboid or diamond shapes (figure 2a), associated to pairs of detector blocks. These are separated with bands whose width depends on the angular gap between consecutive detectors.

A. Crystal penetration

The effect of DOI in the scintillator crystals is also modeled. Scatter in the crystal array has not been considered in the current version of the simulator in benefit of the speed of simulation. The interaction of the gamma ray within the detector is modeled with the expression:

$$N(x) = N(0)e^{-\mu x} \tag{1}$$

where N(0) is the incident number of photons, and μ the linear attenuation factor. The probability density of attenuation in crystal as a function of the penetration distance is:

$$pdf(x) = \mu e^{-\mu x} \tag{2}$$

and the probability of attenuation in crystal:

$$\text{Prob}[X \le x] = \int \mu e^{-\mu x} dx = 1 - e^{-\mu x} \tag{3}$$

In order to reproduce this effect in the simulator, pseudo-random numbers are generated according to the expression (3) from a uniform distribution, using the inverse function method.

IV. Sinogram Mode Rebinning

The 2D filtered backprojection (FBP) requires direct sinograms or 3D to 2D rebinning using SSRB, MSRB, or FORE [4] algorithms. When storing the recorded data as a sinogram, in order to avoid resolution degradation, the minimum size of the sinogram is a function of the number and size of scintillator crystals, as well as of the distance between opposite detectors. The angular bin used is:

$$\Delta\phi_d = \arctan\left(\frac{2d_d}{D + d_m}\right) \tag{4}$$

where d_d is the separation between crystals in the transaxial plane, d_m the mean value of depth of interaction length, and D the distance between opposite detectors.

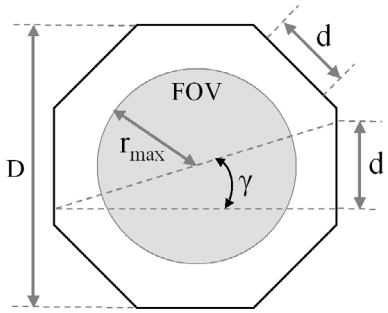

Fig 3. Axial diagram of proposed geometry. The transaxial FOV radius (r_{max}) can be observed.

In an octagonal configuration with twelve pairs of detectors in coincidence, the radius of the transaxial FOV (r_{max}) is determined by the following formula:

$$r_{\max} = \left(\frac{d}{2}\right)\frac{\sin\left(\gamma + \pi/8\right)}{\sin\left(\pi/8\right)} \qquad \gamma = \arctan(d/D) \tag{5}$$

where γ is the arc tangent between the detector length in the transaxial view d, and the distance between opposite detectors D (figure 3).

With this maximum distance and denoting as N_d the number of crystals in a detector block row, the recommended radial dimension of *2D* sinograms is:

$$N(s) = \left\lceil (2N_d - 1)\frac{\sin\left(\gamma + \pi/8\right)}{\sin\left(\pi/8\right)} \right\rceil \tag{6}$$

As sinogram rebinning creates different number of lines of response (LORs) per bin (figure 4a) and sensitivity (figure 4b), the corresponding data correction masks must be computed (figure 4c,d).

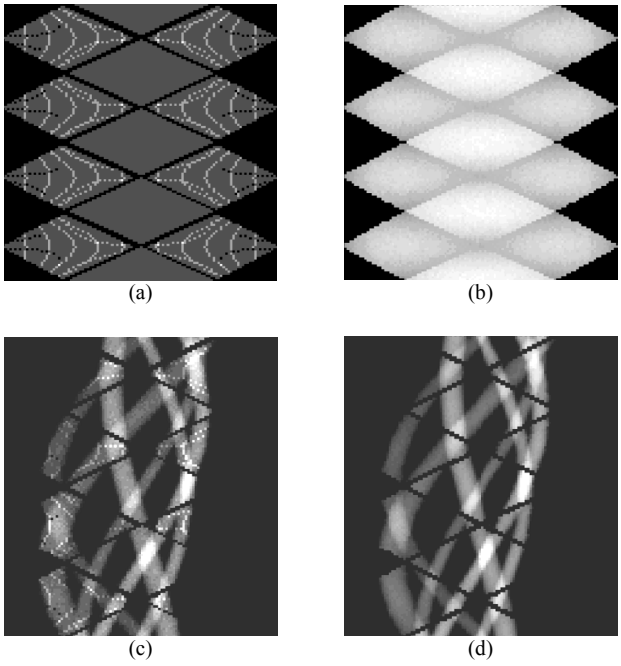

Fig 4. (a) Sinogram correction mask by number of LOR per voxel, (b) correction mask by sensitivity, (c) example of 2D sinogram without sensitivity correction, (d) corrected sinogram.

V. Image Reconstruction

On corrected sinograms FBP reconstruction can be applied, but the presence of bands and zones without registered activity (incomplete sinograms) leads to the generation of significant artifacts in the reconstructed images [5].

Iterative image reconstruction (IIR) algorithms based on statistical models are not significantly affected by the missing data in some projections (i.e., incomplete sinograms). In addition, 3D data can be processed directly in histogram mode, taking advantage of the highest sensitivity in 3D acquisition mode without septa.

A maximum-likelihood expectation-maximization (MLEM) IIR algorithm with Bayesian regularization [6] has been implemented in this work. 2D and 3D versions are available for the proposed octagonal geometry. This algorithm follows the next iterative scheme:

$$x^{k+1}(i) = x^{k}(i)\left(\sum_{j=1}^{J} a(i,j)\frac{y(j)}{\tilde{y}^{k}(j)}\right) \quad (7)$$

where in each iteration k, the i voxel value is updated, being $y(j)$ the acquired projection for the line of response j, and:

$$\tilde{y}(j) = \sum_{i=1}^{I} x(i)a(i,j) \quad (8)$$

the estimated projection, calculated from the probability $a(i,j)$ that an event generated in voxel i is detected in LOR j. The quality of the reconstructed images depends decisively on the accuracy of the calculation of this system matrix. After each iteration a Gaussian regularization filter is applied [6].

In the 3D case the ordered subsets expectation maximization (OSEM) algorithm has been implemented [7]. In 2D, the MLEM reconstruction takes about one second per slice and iteration and does not require the use of accelerated methods.

A. System matrix generation

The system matrix $a(i,j)$ can be computed analytically, approximating the probability of an event generated in voxel i and detected in LOR j, by an estimation of the volume of intersection between the voxel and the tube of response (TOR) j. These models, however, do not consider other physical effects (e.g., DOI, scattering, etc.)

Monte Carlo simulation is an alternative method for the calculation of the system matrix [6]. Depending on the modeled physical processes, this matrix can be more or less realistic. The proposed simulator can be used to create system matrices in 2D and 3D. The main variables are the voxel size and the number of events generated in each of them.

The simulated data are stored in sparse matrix format, since most of the probabilities are zero or have negligible values. The 3D case is especially expensive in processing time. For detector blocks of 30x30 crystals and an image size of 128x128x64 voxels, the system matrix has more than 10^{13} elements. Nevertheless it is only necessary to perform this calculation for each geometric configuration once.

In order to reduce the computation time, the 3D system matrix can be calculated by first computing the values on the voxels of the central transaxial slice and applying the symmetries in the axial axis to obtain the values for the rest of the voxels in the image volume.

The time needed to generate a 3D system matrix having 128x128x64 voxels with axial symmetries is in the order of 50 hours (generating $4{\cdot}10^6$ events per voxel in a 2 GHz Pentium IV PC computer).

VI. Results

A. Sensitivity measurement

The sensitivity (geometrical and crystal intrinsic efficiency) of the proposed tomograph design has been estimated. In figure 5, transaxial views of the sensitivity image obtained for different separations between opposite detectors can be observed. As this separation increases, the transaxial FOV size increases at the cost of losing sensitivity. The sensitivity image presents characteristic patterns, due to the presence of gaps. A detector block size of 48x48x12 mm^3 has been used in this simulation.

B. Reconstructions: 3D and 2D algorithms

Figure 6 shows a comparison between iterative reconstructions in 2D and 3D modes. There are 35x30 LSO crystals in each detector block, each of size 1.6x1.6x12 mm^3 and a attenuation constant of 0.833 mm^{-1}.

The separation between opposite detectors is 141.05 mm, with an angular gap of 1.69 degrees between consecutive detector blocks. The transaxial FOV diameter in this octagonal configuration is 105.71 mm.

A *Derenzo-type* phantom has been simulated. Spheres with diameters between 4 and 1.5 mm are situated in the central transaxial plane, with 50 mm of maximum separation from the center of the FOV.

Figure 6a shows a 3D-OSEM reconstruction of a phantom without including DOI in the simulation of the coincidence data detection. 7 subsets and 4 iterations have been used, with a grid of 128x128x60 voxels. In figure 6b, the simulation of the crystal penetration has been included in the data acquisition, but sinograms are not corrected for DOI. As a result, a degradation of spatial resolution is observed in the reconstructed images.

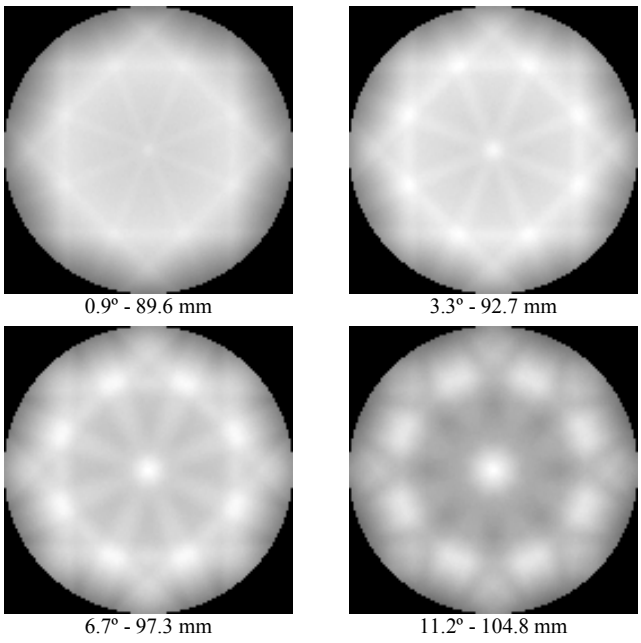

Fig 5. Sensitivity images in the transaxial plane for different FOV diameters. Captions show the angular gap between the edges of two adjacent blocks and the FOV diameter. The images are not represented in the same scale.

Figure 6c shows a 2D-MLEM reconstructed image after 20 iterations without including DOI simulation and figure 6d shows a 2D-MLEM reconstruction where DOI simulation has been included in the data generation process. There is significant improvement in the image quality in the 3D mode, due to the increased sensitivity in comparison to the 2D case.

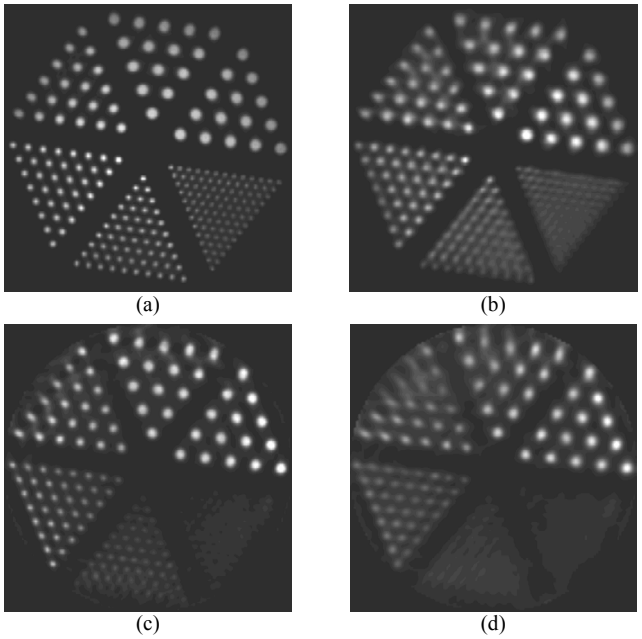

Fig 6. Results for iterative reconstruction of *Derenzo-type* phantom: (a) 3D-OSEM, 7 subsets, 8 iterations, without DOI simulation, (b) 3D-OSEM, 7 subsets, 8 iterations with DOI simulation (no correction or measurement), (c) 2D-MLEM. 20 iterations without DOI simulation, (d) 2D-MLEM, 20 iterations with DOI simulation.

C. Reconstructions: System matrix inaccuracies

Figure 7 shows results from the iterative reconstruction of simulated coincidence data, where inaccuracies in the system matrix calculation have been introduced.

In figure 7a the correct system matrix is used. In figure 7b, the reconstruction is performed using a system matrix corresponding to an octagonal geometry slightly different from the one used for the data generation from the phantom distribution (an additional separation of 10 mm between the detectors located in opposite faces). The degradation of the resulting images is clearly visible.

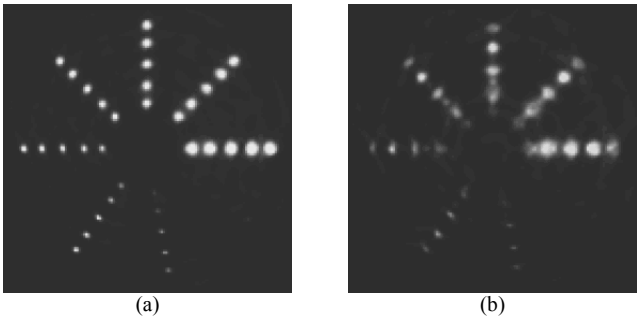

Fig 7. (a) 2D-MLEM Reconstruction of phantom simulated in a octagonal tomograph, (b) 2D-MLEM reconstruction in which a non adjusted system matrix has been used, with significant degradation in the image quality.

VII. Conclusions

We have studied the main performance characteristics of an octagonal small animal PET tomograph using a Monte Carlo simulator and iterative image reconstruction methods.

Octagonal tomograph configurations represent a good compromise between design simplicity, low cost and good sensitivity in comparison to small animal PET scanners employing rotating detector blocks or full rings. Separating the detector blocks can increase the FOV diameter. In that case iterative image reconstruction algorithms can produce images that are not affected by the presence of gaps.

The simulations are efficient enough to allow the relatively fast and accurate pre-calculation of the probability system matrices. The importance of the accuracy in the system matrix calculation has been shown. The depth of interaction for such small-scale geometries represents a crucial factor that adversely affects image resolution and should be taken carefully into consideration for optimal system performance.

The simulator developed can be easily adapted to non-octagonal geometries, and future implementations will include other physical effects (mainly scatter, randoms and attenuation).

VIII. Acknowledgments

This work has been partly founded by the Spanish Ministry of Science & Technology, (TIC 2001-0175-C03) and by *Red Temática IM3* from Spanish Health Ministry (G03/185).

IX. References

[1] K.P. Schäfers, "Imaging Small Animals with Positron Emission Tomography", *Nuklearmedizin*, vol 42, no. 3, pp. 86-89, June 2003.

[2] A.F Chatziioannou, "Molecular Imaging of Small Animals with dedicated PET Tomographs", *Eur. J. Nucl. Med.*, vol. 29, no. 1, pp. 98-114, Jan. 2002.

[3] J. Seidel, J.J Vaquero and M.V Green, "Resolution Uniformity and Sensitivity of the NIH Atlas Small Animal PET Scanner: Comparison to Simulated LSO Scanners Without Depth-of-Interaction Capability", *IEEE Trans. Nucl. Sci.*, vol. 50, no. 5, pp. 1347-1350, Oct. 2003.

[4] M. Defrise, P.E Kinahan, D.W. Townsend, C. Michel, M. Sibomana and D.F. Newport, "Exact and Approximate Rebinning Algorithms for 3-D PET Data", *IEEE Trans. Med. Imag.*, vol. 16, no. 2, pp. 145-158, Apr. 1997.

[5] J.E Ortuño, J.J Vaquero, G. Kontaxakis, A. Santos and M. Desco, "Design of a High Resolution Small Animal Octagonal PET Scanner: Preliminary Studies", *Mol. Imag. Biol*, vol. 5, no. 3, pp. 120-121, May/June 2003.

[6] G. Kontaxakis, L.G. Strauss, T. Thireou, M.J. Ledesma-Carbayo, A. Santos, S.A. Pavlopoulos and A. Dimitrakopoulou-Strauss, "Iterative Image Reconstruction for Clinical PET Using Ordered Subsets, Median Root Prior, and Web-Based Interface", *Mol. Imag. Biol.*, vol. 4, no. 3, pp. 219-231, May-June 2002.

[7] H.M. Hudson and R.S. Larkin, "Accelerated image reconstruction using ordered subsets of projection data", *IEEE Trans. Med. Imag*., vol. 13, no. 4, pp. 601-609, Dec. 1994.